Electronic Supplementary Material (ESI) for Environmental Science: Nano.

Few-layered mesoporous graphene for high-performance toluene adsorption and regeneration

Yaling Wang,[a] Zehui Li,[a] Cheng Tang,[b] Haixia Ren,[a] Qiang Zhang,[a] Mo Xue,[a] Jin Xiong,[c] Dongbin Wang,[a] Qian Yu,[a] Zhiyuan He,[d] Fei Wei [b] and Jingkun Jiang *[a]

[a] State Key Joint Laboratory of Environment Simulation and Pollution Control, School of Environment, Tsinghua University, Beijing 100084, China

[b] Beijing Key Laboratory of Green Chemical Reaction Engineering and Technology, Department of Chemical Engineering, Tsinghua University, Beijing 100084, China.

[c] Institute of Process Engineering, Chinese Academy of Sciences，Beijing 100190, China.

[d] Key Laboratory of Green Printing, Institute of Chemistry, Chinese Academy of Sciences, Beijing 100190, China

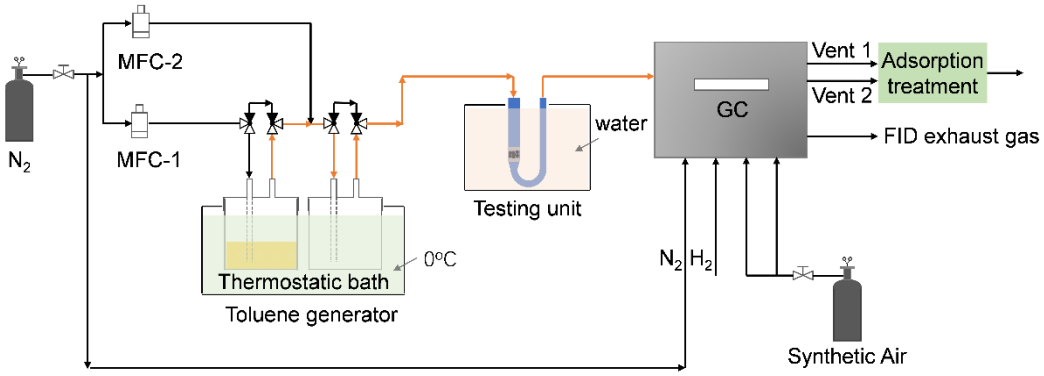

Fig. S1 The home-made setup for adsorption and desorption test of toluene. Toluene generator was kept in a thermostatic bath (0°C) and required concentration was obtained by controlling two flows of saturated gas (MFC–1) and diluent gas (MCF–2). Testing unit consists of U-shape quartz adsorption tube and temperature control system. Adsorbent (graphene materials) was loaded into U-shape quartz tube and sandwiched between silica wool. And then U-shape quartz adsorption tube was kept in the water bath. Temperature of testing unit was controlled at 28.0°C for adsorption test and 95.0°C for desorption test. Detection unit is equipped with a GC with FID and temporal resolution reaches 142 seconds for a record.

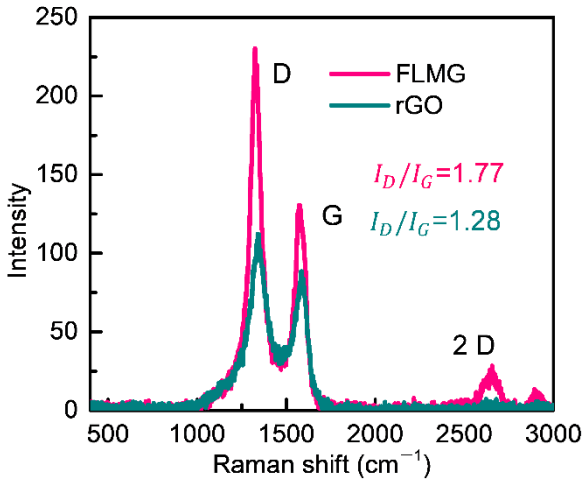

Fig. S2 The Raman spectra of FLMG and rGO. G peak at ~1580 cm^{-1} represents the sp^2 in-plane stretching vibration. G peak of FLMG has a specific red shift at 1574 cm^{-1} compared to that of rGO at 1586 cm^{-1}. It is attributed to the strain of bended structure in nanocages. The D peak at ~1350 cm^{-1} characterizes defects, i.e., sp^3, vacancies or grain boundaries/edges, wrinkle and so on. FLMG with higher value of I_D/I_G indicates more defects than rGO.

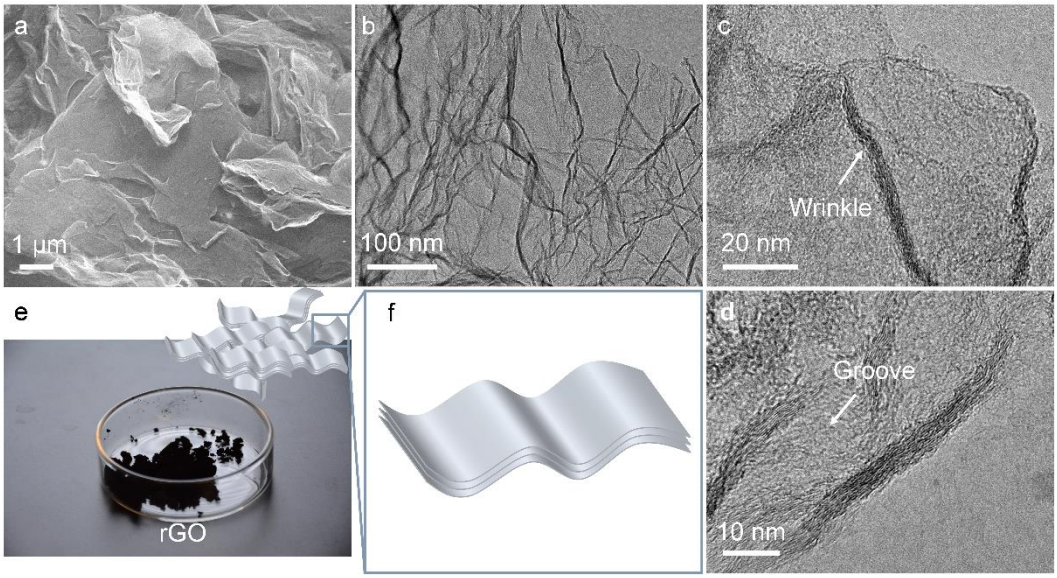

Fig. S3 The randomly aggregated and stacking morphology of nanosheets of rGO. Nanosheet of rGO presents transparent silk-like feature with winkles and grooves.

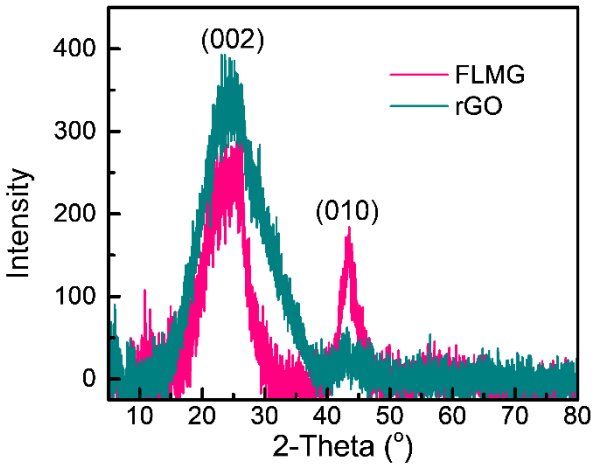

Fig. S4 XRD pattern of FLMG and rGO. The XRD spectra show C (002) diffraction peak at 2-theta = 24.4° and C (010) diffraction peak at 2-theta = 43.5°, indicating the interlayer distance between graphene layers and a short-range order of stacked graphene layers, respectively. According to Bragg's equation, rGO has an interlayer distance of 0.36 nm, while interlayer distance of FLMG appears a little dispersed from 0.34 to 0.39 nm.

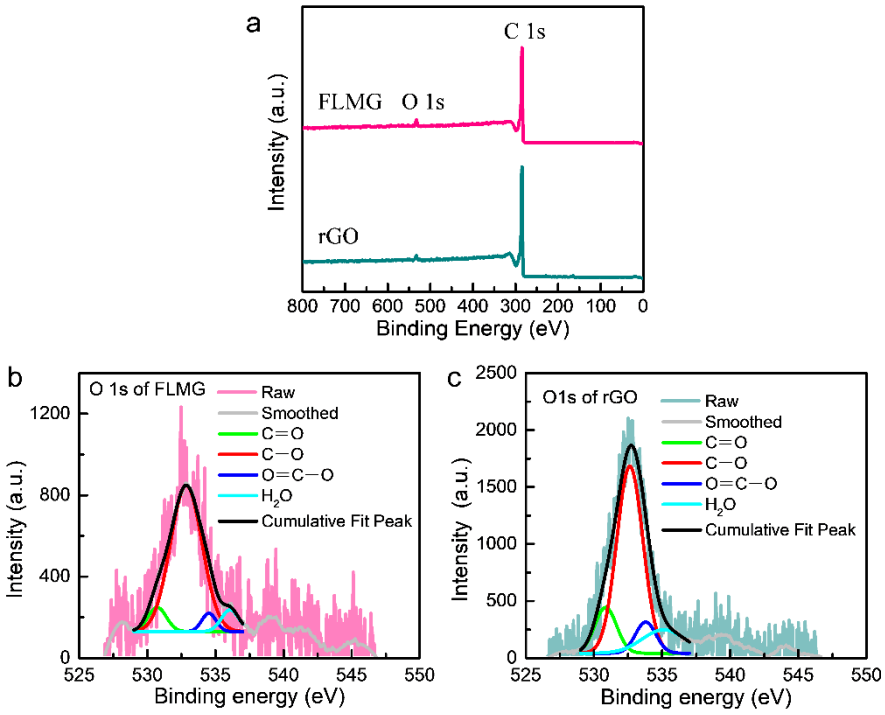

Fig. S5 XPS spectra of FLMG and rGO. Both spectra show a pronounced C 1s peak at 284.7 eV with a small amount of O. Fine O 1s spectra of FLMG and rGO are shown in b and c. XPS survey results confirm absence of Mg element (if Mg exist, the peak of Mg 2p is at 50.8 eV).

Table S1 Pore property of graphene materials by NL-DFT method from N_2 adsorption branch. Total volume refers to the measurement until P/P_0=0.99 and pore sizes extend to 100 nm.

	Pore volume					SSA			
	Total	Micropore		Mesopore	Macropore	BET surface area	Micropore	Mesopore	Macropore
	$cm^3 g^{-1}$	$cm^3 g^{-1}$	v%	v%	v%	($m^2 g^{-1}$)	%	%	%
FLMG	2.70	0.33	12	84	4	1990	36	64	~ 0
rGO	2.56	0.11	4	62	34	652	37	57	6

Table S2 Adsorption capacities for toluene and SSAs of porous materials from references

Materials	**SSA ($m^2 g^{-1}$)**	**Adsorption capacity**	**Adsorption condition**	**References**
Graphene-based				
rGO nanosheet	392	149 mg g^{-1}	Liquid phase, pH 7, C_0 25 ~ 200 mg L^{-1}	1
GO and rGO	236 and 293	240.6 mg g^{-1} and 304.4 mg g^{-1} (breakthrough times of 50-70 min)	50.0 ppm, GO or rGO (500.0 mg),	2
Mesoporous graphene	531 ~ 746	< 263 mg g^{-1}	Volatilization of standard solution	3
ZIF-8/GO (2-25 wt% of GO)	359 ~ 1237	59 ~ 123 mg g^{-1}	—	4
Cu-BTC@GO (2–10 wt% of GO)	1207 ~ 1363	< 100 mg g^{-1} (at $P/P_0 = 0.01$)	Adsorption isotherms of toluene	5, 6
rGO-MW-KOH	326 ~ 491	6 ~ 13 mg g^{-1} (weigh of rGO-MW-KOH)	30 ppm, adsorbent depositing on polypropylene fiber network	7
Steam-activated graphene aerogels	830 ~ 1230	60 mg g^{-1} (at $P/P_0 = 0.055$)	Adsorption isotherms	8
Electrospun graphene oxide/carbon composite nanofibers (3 and 6 wt% GO)	473 ~ 660	< 150 mg g^{-1}, P/P_0=0.01	Adsorption isotherms of benzene	9
3D graphene-based macrostructures	100 ~ 750, 1200	—	Energy field, adsorption	10-12
GO scaffold and rGO/PDMS scaffold (freezing-drying)	Macroscopic scaffold	22 g g^{-1} and 66 g g^{-1}	Liquid solvent, swelling	13
Materials	**SSA ($m^2 g^{-1}$)**	**Adsorption capacity**	**Adsorption condition**	**References**

Nanoporous graphene	410	123 g g^{-1}	Liquid phase	[14]
3D GO sponge	48		Water-soluble dyes	[15]
3D hierarchical porous graphene aerogels	237	21 ~71 g g^{-1}	Liquid solvent	[16]
Active carbon (AC)-based				
Commercial AC	932 ~ 952	265 ~ 282 mg g^{-1}	Active carbon 20 g, 2000 ppm	[17]
Commercial AC	1146	128 mg g^{-1}	500 ppm, 55 mg	[18]
AC(s)	656 ~ 2478	170 ~ 560 mg g^{-1}	200 ppm, 70 ~ 110 mg	[19]
AC	990	88 mg g^{-1} at P/P_0=0.1	isotherm	[20]
AC	571 ~ 1285	< 230 mg g^{-1} at 100 kPa	Static adsorption by volumetric method	[21]
AC	502 ~ 1128	46 ~ 138 mg g^{-1}	500-1000 ppm,100 mg	[22]
R-CAFS and AC40	1255 and 1030	210 mg g^{-1}, 160 mg g^{-1}	0.435 mmol L^{-1} solvent, 20 g	[23]
Acid-treated ACs	1067 ~ 840	104 ~ 123 mg g^{-1}	150 ppm, 6 L min^{-1}	[24]
ACs (biomass)	571 ~ 1284	< 46 mg g^{-1} at P=5 kPa	isotherm	[21]
Activated carbon fibers	1026 ~ 1826	270 ~ 530 mg g^{-1}	200 ppm,75 mg	[25]
Spherical activated carbon	1291 ~ 2586	310 ~ 460 mg g^{-1}	200 ppm, 250 mg	[26]
Activated carbon monolith	615	180 mg g^{-1} at P=1 kPa	isotherm	[27]
Mesoporous carbon	1762	< 270 mg g^{-1} at P(benzene) <1 kPa	isotherm	[28]
Biochars	0.1 ~ 388	13 ~ 63 mg g^{-1}	5 mg	[29]
Zeolites				
MCM-41	1154	199 mg g^{-1}	500 ppm, 55 mg	[18]
SBA-15	730 ~ 430	119 ~ 153 mg g^{-1}	500 ppm, 55 mg	[18]
Silica gel Q3	725	102 mg g^{-1}	500 ppm, 55 mg	[18]
Materials	**SSA (m^2 g^{-1})**	**Adsorption capacity**	**Adsorption condition**	**References**

Zeolite HY	732	94 mg g^{-1}	500 ppm, 55 mg	[18]
SBA-15 fiber	760 ~ 880	0.08 ~ 0.1 mg g^{-1}	500 ppm, 100 mg	[30]
Dealuminated Y-zeolite	704	138 mg g^{-1} at P=1kPa	5000 ppm, 10 mL min^{-1}	[31]
Diatomite/MFI-type zeolite	290	40 mg g^{-1} at P/P_0=0.1 benzene	isotherm	[32]
Silica Gel	535	54 mg g^{-1} at P/P0=0.1	isotherm	[20]
13x zeolite	440	8 mg g^{-1} at P/P0=0.1	isotherm	[20]
SBA-15 and Phenyl-SBA-15	698 and 506	83 mg g^{-1}, 60 mg g^{-1}	1000 ppm (benzene), 100 mg	[33]
MCM-41 and Phenyl-MCM-41	1088 and 950	94 mg g^{-1}, 83 mg g^{-1}	1000 ppm (benzene), 100 mg	[33]
MCM-48 and Phenyl-MCM-48	1210 and1164	90 mg g^{-1}, 72 mg g^{-1}	1000 ppm (benzene), 100 mg	[33]
KIT-6 and Phenyl-KIT-6	912 and 751	116 mg g^{-1}, 108 mg g^{-1}	1000 ppm (benzene), 100 mg	[33]
Zeolite samples	23 ~ 870	0.3 ~ 200 mg g^{-1}	216 ppm, 404 mL min^{-1}	[34]
Phenyl- KIT-6	761 ~ 899	170 ~ 184 mg g^{-1}	1000 ppm, 100 mg	[35]
KIT-6	944	177 mg g^{-1}	1000 ppm, 100 mg	[35]
MOFs				
MOF-177	2970	140 mg g^{-1} at P/P_0=0.1	isotherm	[36]
HKUST-1	907	165 mg g^{-1} at P/P_0=0.01	isotherm	[37]
MIL-101	3483	120 mg g^{-1} at P/P_0=0.01	isotherm	[37]
Cu-BTC	1188	6.2 mmol/g at P/P_0=1	isotherm	[6]
UiO-66	1335	151 mg g^{-1}	1000 ppm, 200 mg	[38]
Micro-mesoporous UiO-66	1232 ~ 999	226 ~ 394 mg g^{-1}	1000 ppm, 200 mg	[38]
UiO-66 (PVP	1162 ~ 1134	173 ~ 259 mg g^{-1}	1000 ppm, 200 mg	[39]
UiO-66 (CTAB)	1103 ~ 962	177 ~ 275 mg g^{-1}	1000 ppm, 200 mg	[40]
MIL-101	3980	< 400 mg g^{-1} at P/P_0=0.05	isotherm	[41]
Materials	**SSA (m^2 g^{-1})**	**Adsorption capacity**	**Adsorption condition**	**References**

MIL-101	2728	2115 mg g^{-1}	1 ppm, 200 mg, 600 mL min^{-1}	[42]
MIL-53	951	730 mg g^{-1}	1 ppm, 200 mg, 600 mL min^{-1}	[42]
CPM-5	1140	389 mg g^{-1}	1 ppm, 200 mg, 600 mL min^{-1}	[42]
ZIF-8	1305 ~ 822	72 ~ 382 mg g^{-1}	1000 ppm, 100 mg	[43]
UiO-66-NH_2	1250	252 mg g^{-1}	99 ppm, 5 mg	[44]
UiO-66	1414	166 mg g^{-1}	99 ppm, 5 mg	[44]
MOF-199	1237	159 mg g^{-1}	99 ppm, 5 mg	[44]
ZIF-67	1401	224 mg g^{-1}	99 ppm, 5 mg	[44]
MOF-5	424	33 mg g^{-1}	99 ppm, 5 mg	[44]
MIL-101(Fe)	377	98 mg g^{-1}	99 ppm, 5 mg	[44]
Others				
SWNT	1347 ~ 897	240 ~ 383 mg g^{-1}	225 ~ 260 ppm	[45]
MWNT	10 ~ 187	8.9 ~ 11 mg g^{-1}	225 ~ 260 ppm	[45]
Dichloroalkane hyper-cross-linked polymer	240 ~ 1220	0.9 ~ 0.2 cm^3 g^{-1} at P/P_0 = 0.05		[46]

Calculation of relative pressure

The Antoine equation is a semi-empirical correlation describing the relation between saturated vapor pressure and temperature for pure components. The expression is following

$$\log_{10}P=A-\frac{B}{t+C} \quad \text{(S1)}$$

Where, P is the saturated vapor pressure (mmHg); t is the temperature (^{o}C); for toluene, the values of three parameter of A, B and C are 6.95464, 1344.800 and 219.482.

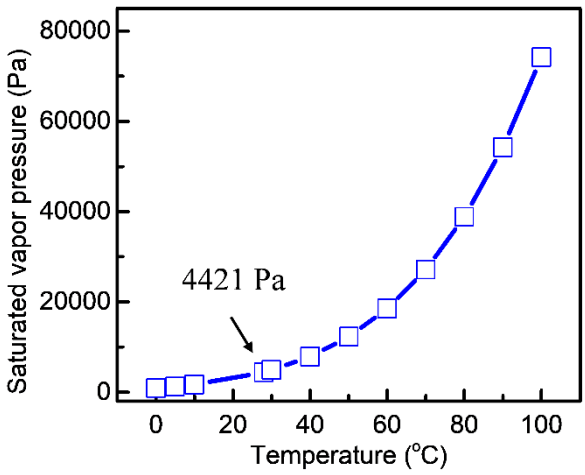

Fig. S6 The relation curve of saturated vapor pressure of toluene and temperature.

The partial pressure of toluene (120 ppm) is 12.16 Pa. and saturated vapor pressure of toluene at 28°C is 4421 Pa. The relative saturated pressure of toluene is 0.003.

Table S3 Parameters for adsorbed toluene in graphitic slit-pore from Do et al.'s work[47]

Pore width (nm)	V_{acc} (nm^3) [a]	V_{phy} (nm^3) [b]	V_{He} (nm^3) [c]	R_{phy} [d]	R_{He} [e]	Density of adsorbed toluene		
						(kmol m^{-3}) [f]	(kmol m^{-3}) [g]	(g cm^{-3}) [h]
0.8	3.93	80.00	70.15	0.0491	0.0560	4.8	97.7	9.0
1	19.55	100.00	89.11	0.1955	0.2194	3.9 [i]	19.7	1.8
1.2	38.79	120.00	97.17	0.3233	0.3992	2.9 [i]	9.0	0.8
1.6	78.40	160.00	138.36	0.4900	0.5666	1.0	2.0	0.2
2	118.44	200.00	179.09	0.5922	0.6613	0.5	0.8	0.1
3	218.10	300.00	281.60	0.7270	0.7745			

[a] The accessible pore volume is defined as the volume accessible to the center of a particle at zero loading and is determined by the Monte Carlo method of integration.

[b] The physical pore volume is defined as the volume between the plane passing through the centers of carbon atoms of the outermost layer of one wall and the corresponding plane of the opposite wall.

[c] The pore volume is determined by GCMC simulation of helium adsorption at 1 atm and room temperature.

[d] The ratio of accessible pore volume to the physical pore volume.

[e] The ratio of accessible pore volume to the pore volume determined by helium adsorption in the [c] term.

[f] Density of adsorbed toluene (based on the physical pore volume) vs relative pressure from adsorption/desorption isotherms at P/P_0 (0.003).

[g] Density of adsorbed phase calculated from the [f] term and [d] term.

[h] Density of adsorbed phase transformed from [g] term.

[i] The value obtained by interpolation using the other values of the [f] term.

Table S4 An estimation of toluene amount in micropore of FLMG and rGO

Materials	Pore width (nm)	Pore volume from NL-DFT ($cm^3\ g^{-1}$)	Accessible pore volume ($cm^3\ g^{-1}$) [j]	Toluene in pore (mg g^{-1}) [k]	Total toluene in pore (mg g^{-1}) [l]
FLMG	0.8	0.091	0.005	45.7	95.5
	1	0.000	0.000	0.0	
	1.2	0.111	0.044	36.6	
	1.6	0.121	0.069	12.9	
	2	0.006	0.004	0.3	
	Micropore volume	0.33			
rGO	0.8	0.022	0.001	11.1	34.0
	1	0.000	0.000	0.0	
	1.2	0.060	0.024	19.6	
	1.6	0.031	0.018	3.3	
	2	0.000	0.000	0.0	
	Micropore volume	0.11			

[j] The accessible pore volume is obtained from pore volume from NL-DFT ($cm^3\ g^{-1}$) and [e] term.

[k] Amount of adsorbed toluene in pore is calculated from [j] term and [h] term.

[l] Total toluene in pore is the sum of the [k] term.

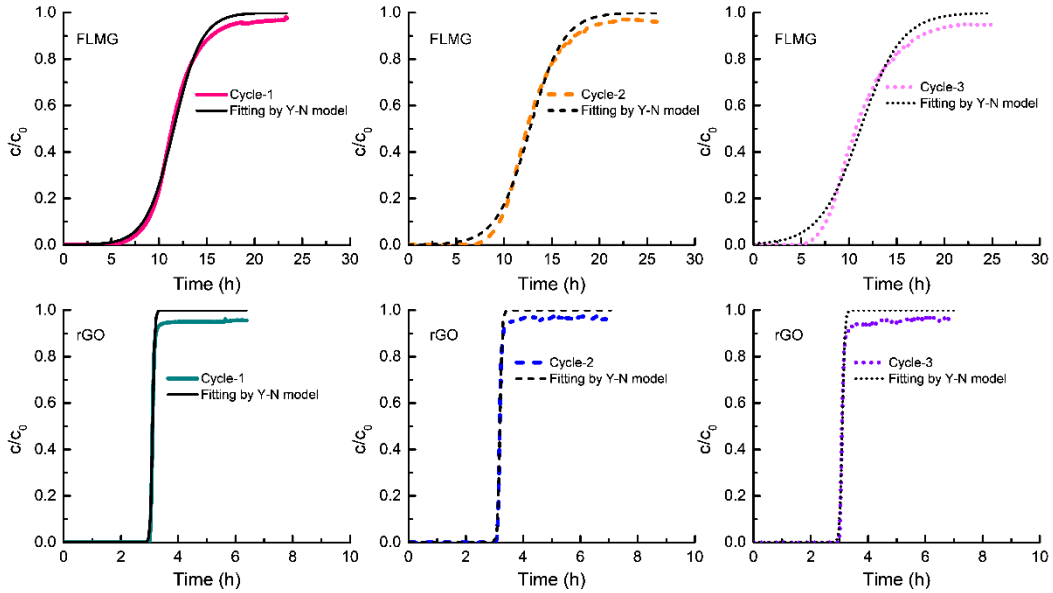

Fig. S7 The breakthrough curves of FLMG and rGO during three cycles of adsorption fitted by Yoon-Nelson model.

The Yoon-Nelson[48] model is expressed as following:

$$t = \tau_{1/2} + \frac{1}{k'} \ln\left(\frac{c}{c_0 - c}\right) \quad \text{(S2)}$$

$$k = k' \tau_{1/2} \quad \text{(S3)}$$

where c and c_0 are the effluent and influent concentration of toluene at time t (h), $\tau_{1/2}$ (h) is the half breakthrough time when $c = c_0/2$, k' (h^{-1}) is the rate constant representing the toluene diffusion characteristic in the fixed bed. k is the proportionality constant. This model is based on the assumption that the rate of decrease in the probability of adsorption for each adsorbate molecule is proportional to the probability of adsorbate adsorption and the probability of adsorbate breakthrough on the adsorbent.

The fraction form is

$$f(t) = \frac{c}{c_0} = \frac{1}{1 + e^{-k'(t - \tau_{1/2})}} \quad \text{(S4)}$$

Table S5 Fitting parameters for breakthrough curves by a Yoon-Nelson model

FLMG	Y-N model: $f(t)=\frac{c}{c_0}=\frac{1}{1+e^{-k'(t-\tau_{1/2})}}$			
Adsorption	Parameters	Value	Standard Error	R^2
Cycle 1	$\tau_{1/2}$ (h)	11.54	0.02	0.996
	k' (h^{-1})	0.68	0.01	
Cycle 2	$\tau_{1/2}$ (h)	12.71	0.02	0.995
	k' (h^{-1})	0.57	0.01	
Cycle 3	$\tau_{1/2}$ (h)	11.21	0.03	0.989
	k' (h^{-1})	0.47	0.01	
FLMG	$\tau_{1/2}$=11.8 ± 0.8 (h); k' = 0.6 ± 0.1 (h^{-1}), $k=k'\tau_{1/2}$=6.8 ± 1.4			
rGO	Y-N model: $f(t)=\frac{c}{c_0}=\frac{1}{1+e^{-k'(t-\tau_{1/2})}}$			
Adsorption	Parameters	Value	Standard Error	R^2
Cycle 1	$\tau_{1/2}$ (h)	3.11	0.00	0.996
	k' (h^{-1})	28.39	2.46	
Cycle 2	$\tau_{1/2}$ (h)	3.19	0.00	0.997
	k' (h^{-1})	27.36	1.70	
Cycle 3	$\tau_{1/2}$ (h)	3.10	0.00	0.994
	k' (h^{-1})	24.27	1.96	
rGO	$\tau_{1/2}$=3.1 ± 0.1 (h); k' = 26.7 ± 2.1 (h^{-1}); $k=k'\tau_{1/2}$=83.6 ± 7.3			

Micropore filling of N_2

When micropore is filled fully by N_2 at 77 K, the amount of condensed N_2 equals to micropore volume. According the relationship that 1 mL N_2 under standard temperature and pressure (STP) has a condensation volume of 0.001547 mL, the amount of N_2 (STP) filling in the micropore is

$$Q\ (\mathrm{N_2,mL\ STP}) = \frac{\text{amount of condensed } \mathrm{N_2}}{0.001547} = \frac{\text{Micropore volume}}{0.001547} \tag{S5}$$

So, the amounts of N_2 filling in micropore volumes of FLMG and rGO are 213 mL (STP) and 71 mL (STP), respectively. In the form of mole, those are 9.5 mmol for FLMG and 3.2 mmol for rGO per gram adsorbent. Further, the corresponding relative pressure (P/P_0) on the N_2 adsorption isotherms is picked out at 0.0005 for FLMG and 0.00049 for rGO.

Among there, the mole of 1mL N_2 (STP) is calculated as following

$$n = \frac{PV}{RT} = 4.46\times10^{-5}\ \text{mol} \tag{S6}$$

And then the equivalent mass of condensed N_2 is

$$m = nM = 4.46\times10^{-5}\times28 = 1.25\times10^{-3}\ \text{g} \tag{S7}$$

So, the volume of N_2 can be calculated based on that the condensed N_2 has a density of 0.808 g cm^{-3}.

$$V = \frac{m}{\rho} = \frac{1.25\times10^{-3}}{0.808} = 0.001547\ \text{mL} \tag{S8}$$

The adsorption of FLMG for toluene/cyclohexane mixture and toluene/benzene mixture are carried out using mixed standard gases with a concentration of ～100 ppm for each species. The breakthrough curves are illustrated in Fig. S8.

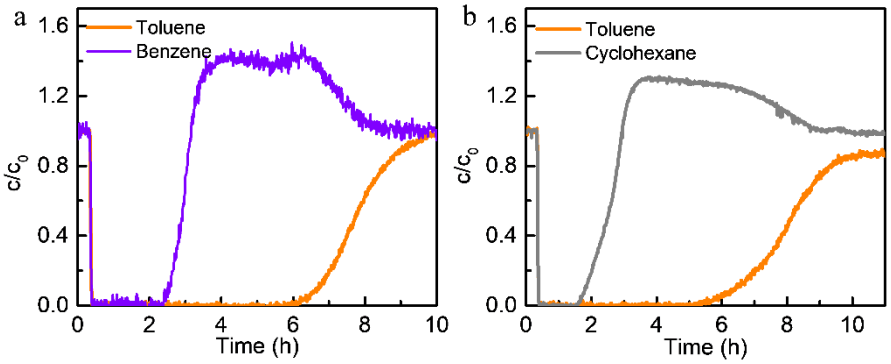

Fig. S8 The breakthrough curves of FLMG for (a) toluene/benzene mixture (toluene 95.8 ppm, benzene 98.0 ppm), (b) toluene/cyclohexane mixture (toluene 104.0 ppm, cyclohexane 95.0 ppm. The flow rate of mixture is 50 mL min^{-1}. The used adsorbent FLMG is 50.0 mg.

During the adsorption of toluene/benzene mixture, the adsorption capacity of FLMG reaches 163.3 mg g^{-1} for toluene, higher than that adsorption capacity of benzene (16.7 mg g^{-1}) with nearly the same concentration. The selective adsorption of FLMG for toluene over benzene is owing to the higher relative saturated vapor pressure (P/P_0) of toluene than benzene [49] (P/P_0 is 0.0022 for toluene with P_0 = 4.42 kPa and P/P_0 is 0.00068 for benzene with P_0 = 14.55 kPa at 28°C) and the larger molecular weight . As for the adsorption of toluene/cyclohexane mixture, the adsorption capacities of toluene and cyclohexane are 184.3 mg g^{-1} and 15.6 mg g^{-1}, respectively. The selective adsorption of FLMG to toluene over cyclohexane is attributed to the strong π-π interaction of toluene with graphene [33].

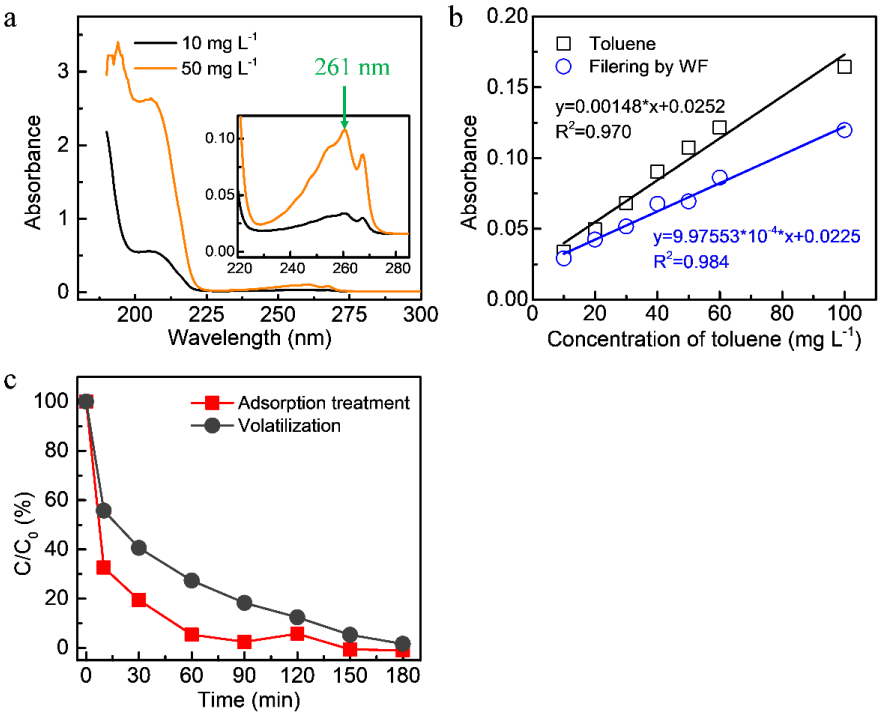

Fig. S9. The adsorption of FLMG for trace toluene in aqueous solution. (a) The wavelength scanning of absorbance of toluene solution (take toluene solution of 10 mg L^{-1} and 50 mg L^{-1} as examples). The wavelength of 261 nm was chosen for quantification of concentration. (b) Standard curve of toluene solution (black fitting line) and the effect of filter performance (blue fitting line). (c) Concentration of toluene solution varies with adsorption time (red dotted line). The volatilization loss of toluene solution is evaluated (dark black dotted line).

An experiment was carried to evaluate the adsorption of trace toluene in aqueous solution by FLMG as following. Firstly, a water solution of toluene (500.0 mg L^{-1}) was prepared and then it was sealed and mixed on a magnetic stirrer overnight. A series toluene solution with different concentration was obtained by diluting above toluene storage solution with ultrapure water. The absorbance values were scanned from 450 nm to 190 nm on UV-visible spectrophotometer (UV2310II, Techcomp. and relative maximum values were picked out at 261 nm. Standard curve plots the absorbance of toluene solution against concentration. For performing the adsorption of FLMG for trace toluene, 10.0 mg FLMG was mixed into 50 ml toluene solution (50 mg L^{-1}) and the mixture was stirred at 200 rpm. 2.3 mL mixture was sampled at certain intervals

and filtered by a syringe filter (polyether sulfone, 0.45μm, ANPEL Co., Ltd.) for absorbance measurement. Considering the volatilization loss, toluene solution without feeding FLMG was evaluated as well. Finally, as the adsorption result revealed in Fig. S9c, the concentration of toluene solution after adsorption by FLMG is lower than that after considering volatilization loss under the same condition, indicating that FLMG can adsorb trace toluene in aqueous solution.

References

1 M. T. Raad, H. Behnejad and M. E. Jamal, Equilibrium and kinetic studies for the adsorption of benzene and toluene by graphene nanosheets: a comparison with carbon nanotubes, *Surf. Interface. Anal.*, 2016, **48**, 117-125.

2 L. Yu, L. Wang, W. Xu, L. Chen, M. Fu, J. Wu and D. Ye, Adsorption of VOCs on reduced graphene oxide, *J. Environ. Sci.*, 2018, **67**, 171-178.

3 J. Lee, M. Kang, I.-K. Shim, D. H. Lee, A. Kim and H. Jung, Pore Parameters-Dependent Adsorption Behavior of Volatile Organic Compounds on Graphene-Based Material, *J. Nanosci. Nanotechnol.*, 2018, **18**, 6995-7003.

4 F. Chu, Y. Zheng, B. Wen, L. Zhou, J. Yan and Y. Chen, Adsorption of toluene with water on zeolitic imidazolate framework-8/graphene oxide hybrid nanocomposites in a humid atmosphere, *RSC Adv.*, 2018, **8**, 2426-2432.

5 B. Szczęśniak, J. Choma and M. Jaroniec, Gas adsorption properties of hybrid graphene-MOF materials, *J. Colloid Interf. Sci*, 2018, **514**, 801-813.

6 Y. Li, J. Miao, X. Sun, J. Xiao, Y. Li, H. Wang, Q. Xia and Z. Li, Mechanochemical synthesis of Cu-BTC@GO with enhanced water stability and toluene adsorption capacity, *Chem. Eng. J.*, 2016, **298**, 191-197.

7 J. M. Kim, J. H. Kim, C. Y. Lee, D. W. Jerng and H. S. Ahn, Toluene and acetaldehyde removal from air on to graphene-based adsorbents with microsized pores, *J. Hazard. Mater.*, 2018, **344**, 458-465.

8 Z.-Y. Sui, Q.-H. Meng, J.-T. Li, J.-H. Zhu, Y. Cui and B.-H. Han, High surface area porous carbons produced by steam activation of graphene aerogels, *J. Mater. Chem. A*, 2014, **2**, 9891-9898.

9 Z. Guo, J. Huang, Z. Xue and X. Wang, Electrospun graphene oxide/carbon composite nanofibers with well-developed mesoporous structure and their adsorption performance for benzene and butanone, *Chem. Eng. J.*, 2016, **306**, 99-106.

10 Y. Shen, Q. Fang and B. Chen, Environmental Applications of Three-Dimensional Graphene-Based Macrostructures: Adsorption, Transformation, and Detection, *Environ. Sci. Technol.*, 2015, **49**, 67-84.

11 Y. Tao, D. Kong, C. Zhang, W. Lv, M. Wang, B. Li, Z.-H. Huang, F. Kang and Q.-H. Yang, Monolithic carbons with spheroidal and hierarchical pores produced by the linkage of functionalized graphene sheets, *Carbon*, 2014, **69**, 169-177.

12 S. Nardecchia, D. Carriazo, M. L. Ferrer, M. C. Gutiérrez and F. del Monte, Three dimensional macroporous architectures and aerogels built of carbon nanotubes and/or graphene: synthesis and applications, *Chem. Soc. Rev.*, 2013, **42**, 794-830.

13 S. Park, S.-O. Kang, E. Jung, S. Park and H. S. Park, Surface modification and partial reduction of three-dimensional macroporous graphene oxide scaffolds for greatly improved adsorption capacity, *RSC Adv.*, 2014, **4**, 899-902.

14 S. Pourmand, M. Abdouss and A. M. Rashidi, Preparation of Nanoporous Graphene via Nanoporous Zinc Oxide and its Application as a Nanoadsorbent for Benzene, Toluene and Xylenes Removal, *Int. J. Environ.Res.*, 2015, **9**, 1269-1276.

15 F. Liu, S. Chung, G. Oh and T. S. Seo, Three-Dimensional Graphene Oxide Nanostructure for Fast and Efficient Water-Soluble Dye Removal, *ACS Appl. Mater.*

Interfaces, 2012, **4**, 922-927.
16 C. Chi, H. Xu, K. Zhang, Y. Wang, S. Zhang, X. Liu, X. Liu, J. Zhao and Y. Li, 3D hierarchical porous graphene aerogels for highly improved adsorption and recycled capacity, *Mater. Sci. Eng.: B*, 2015, **194**, 62-67.
17 L. Li, Z. Sun, H. Li and T. C. Keener, Effects of activated carbon surface properties on the adsorption of volatile organic compounds, *J. Air. Waste. Manage.*, 2012, **62**, 1196-1202.
18 K. Kosuge, S. Kubo, N. Kikukawa and M. Takemori, Effect of Pore Structure in Mesoporous Silicas on VOC Dynamic Adsorption/Desorption Performance, *Langmuir*, 2007, **23**, 3095-3102.
19 M. A. Lillo-Ródenas, D. Cazorla-Amorós and A. Linares-Solano, Behaviour of activated carbons with different pore size distributions and surface oxygen groups for benzene and toluene adsorption at low concentrations, *Carbon*, 2005, **43**, 1758-1767.
20 C.-M. Wang, K.-S. Chang, T.-W. Chung and H. Wu, Adsorption Equilibria of Aromatic Compounds on Activated Carbon, Silica Gel, and 13X Zeolite, *J. Chem. Eng. Data*, 2004, **49**, 527-531.
21 X. Yang, H. Yi, X. Tang, S. Zhao, Z. Yang, Y. Ma, T. Feng and X. Cui, Behaviors and kinetics of toluene adsorption-desorption on activated carbons with varying pore structure, *J. Environ. Sci.*, 2018, **67**, 104-114.
22 A. Martínez de Yuso, M. T. Izquierdo, R. Valenciano and B. Rubio, Toluene and n-hexane adsorption and recovery behavior on activated carbons derived from almond shell wastes, *Fuel Process. Technol*, 2013, **110**, 1-7.
23 M. Popescu, J. P. Joly, J. Carré and C. Danatoiu, Dynamical adsorption and temperature-programmed desorption of VOCs (toluene, butyl acetate and butanol) on activated carbons, *Carbon*, 2003, **41**, 739-748.
24 S.-H. Pak, M.-J. Jeon and Y.-W. Jeon, Study of sulfuric acid treatment of activated carbon used to enhance mixed VOC removal, *Int. Biodeter. Biodegr*, 2016, **113**, 195-200.
25 M. A. Lillo-Ródenas, D. Cazorla-Amorós and A. Linares-Solano, Benzene and toluene adsorption at low concentration on activated carbon fibres, *Adsorption.*, 2011, **17**, 473-481.
26 A. J. Romero-Anaya, M. A. Lillo-Ródenas and A. Linares-Solano, Spherical activated carbons for low concentration toluene adsorption, *Carbon*, 2010, **48**, 2625-2633.
27 F. D. Yu, L. Luo and G. Grevillot, Electrothermal swing adsorption of toluene on an activated carbon monolith: Experiments and parametric theoretical study, *Chem. Eng.Process.*, 2007, **46**, 70-81.
28 G. Wang, B. Dou, Z. Zhang, J. Wang, H. Liu and Z. Hao, Adsorption of benzene, cyclohexane and hexane on ordered mesoporous carbon, *J. Environ. Sci.*, 2015, **30**, 65-73.
29 X. Zhang, B. Gao, Y. Zheng, X. Hu, A. E. Creamer, M. D. Annable and Y. Li, Biochar for volatile organic compound (VOC) removal: Sorption performance and governing mechanisms, *Bioresource. Technol.*, 2017, **245**, 606-614.

30 S. Kubo and K. Kosuge, Salt-Induced Formation of Uniform Fiberlike SBA-15 Mesoporous Silica Particles and Application to Toluene Adsorption, *Langmuir*, 2007, **23**, 11761-11768.
31 D.-G. Lee, J.-H. Kim and C.-H. Lee, Adsorption and thermal regeneration of acetone and toluene vapors in dealuminated Y-zeolite bed, *Sep. Purif. Technol.*, 2011, **77**, 312-324.
32 W. Yu, L. Deng, P. Yuan, D. Liu, W. Yuan and F. Chen, Preparation of hierarchically porous diatomite/MFI-type zeolite composites and their performance for benzene adsorption: The effects of desilication, *Chem. Eng. J.*, 2015, **270**, 450-458.
33 B. Dou, Q. Hu, J. Li, S. Qiao and Z. Hao, Adsorption performance of VOCs in ordered mesoporous silicas with different pore structures and surface chemistry, *J. Hazard. Mater.*, 2011, **186**, 1615-1624.
34 M. Kraus, U. Trommler, F. Holzer, F.-D. Kopinke and U. Roland, Competing adsorption of toluene and water on various zeolites, *Chem. Eng. J.*, 2018, **351**, 356-363.
35 S. Liu, J. Chen, Y. Peng, F. Hu, K. Li, H. Song, X. Li, Y. Zhang and J. Li, Studies on toluene adsorption performance and hydrophobic property in phenyl functionalized KIT-6, *Chem. Eng. J.*, 2018, **334**, 191-197.
36 K. Yang, F. Xue, Q. Sun, R. Yue and D. Lin, Adsorption of volatile organic compounds by metal-organic frameworks MOF-177, *J. Environ. Chem. Eng.*, 2013, **1**, 713-718.
37 F. Xu, S. Xian, Q. Xia, Y. Li and Z. Li, Effect of Textural Properties on the Adsorption and Desorption of Toluene on the Metal-Organic Frameworks HKUST-1 and MIL-101, *Adsorpt. Sci. Technol.*, 2013, **31**, 325-339.
38 X. Zhang, Y. Yang, X. Lv, Y. Wang, N. Liu, D. Chen and L. Cui, Adsorption/desorption kinetics and breakthrough of gaseous toluene for modified microporous-mesoporous UiO-66 metal organic framework, *J. Hazard. Mater.*, 2019, **366**, 140-150.
39 X. Zhang, X. Lv, X. Shi, Y. Yang and Y. Yang, Enhanced hydrophobic UiO-66 (University of Oslo 66) metal-organic framework with high capacity and selectivity for toluene capture from high humid air, *J. Colloid Interf. Sci*, 2019, **539**, 152-160.
40 X. Zhang, Y. Yang, L. Song, J. Chen, Y. Yang and Y. Wang, Enhanced adsorption performance of gaseous toluene on defective UiO-66 metal organic framework: Equilibrium and kinetic studies, *J. Hazard. Mater.*, 2019, **365**, 597-605.
41 K. Yang, Q. Sun, F. Xue and D. Lin, Adsorption of volatile organic compounds by metal–organic frameworks MIL-101: Influence of molecular size and shape, *J. Hazard. Mater.*, 2011, **195**, 124-131.
42 M. Bahri, F. Haghighat, H. Kazemian and S. Rohani, A comparative study on metal organic frameworks for indoor environment application: Adsorption evaluation, *Chem. Eng. J.*, 2017, **313**, 711-723.
43 S. Jafari, F. Ghorbani-Shahna, A. Bahrami and H. Kazemian, Adsorptive removal of toluene and carbon tetrachloride from gas phase using Zeolitic Imidazolate Framework-8: Effects of synthesis method, particle size, and pretreatment of the adsorbent, *Micropor. Mesopor. Mat*, 2018, **268**, 58-68.

44 K. Vellingiri, P. Kumar, A. Deep and K.-H. Kim, Metal-organic frameworks for the adsorption of gaseous toluene under ambient temperature and pressure, *Chem. Eng. J.*, 2017, **307**, 1116-1126.
45 R. H. Gangupomu, M. L. Sattler and D. Ramirez, Comparative study of carbon nanotubes and granular activated carbon: Physicochemical properties and adsorption capacities, *J. Hazard. Mater.*, 2016, **302**, 362-374.
46 M. Ghafari and J. D. Atkinson, Impact of styrenic polymer one-step hyper-cross-linking on volatile organic compound adsorption and desorption performance, *J. Hazard. Mater.*, 2018, **351**, 117-123.
47 N. Klomkliang, D. D. Do and D. Nicholson, Affinity and Packing of Benzene, Toluene, and p-Xylene Adsorption on a Graphitic Surface and in Pores, *Ind. Eng. Chem. Res.*, 2012, **51**, 5320-5329.
48 R. Moradi, J. Karimi-Sabet, M. Shariaty-Niassar and M. A. Koochaki, Preparation and Characterization of Polyvinylidene Fluoride/Graphene Superhydrophobic Fibrous Films, *Polymers*, 2015, **7**, 1444.
49 M. A. Lillo-Ródenas, A. J. Fletcher, K. M. Thomas, D. Cazorla-Amorós and A. Linares-Solano, Competitive adsorption of a benzene–toluene mixture on activated carbons at low concentration, *Carbon*, 2006, **44**, 1455-1463.